



POLITECNICO
MILANO 1863

DIPARTIMENTO DI MECCANICA



Optical characterization of laser coloured titanium under different processing atmospheres

Khafaji, Noor Yasir; Demir, Ali Gökhan; Vitali, Luigi; Fustinoni, Damiano; Niro, Alfonso; Previtali, Barbara; Taha, Ziad A.

This is a post-peer-review, pre-copyedit version of an article published in SURFACE & COATINGS TECHNOLOGY. The final authenticated version is available online at:

<http://dx.doi.org/10.1016/j.surfcoat.2017.04.043>

This content is provided under [CC BY-NC-ND 4.0](https://creativecommons.org/licenses/by-nc-nd/4.0/) license



Optical characterization of laser coloured titanium under different processing atmospheres

Noor Yasir Khafaji¹, Ali Gökhan Demir^{2*}, Luigi Vitali³, Damiano Fustinoni³, Alfonso Niro³, Barbara Previtali², Ziad A. Taha¹

¹ Institute of Laser for Postgraduate Studies, University of Baghdad, Baghdad, Iraq

² Department of Mechanical Engineering, Politecnico di Milano, Via La Masa 1, 20156 Milan, Italy

³ Energy Department, Politecnico di Milano, Via Lambruschini 4, 20156 Milan, Italy

*Corresponding author. aligokhan.demir@polimi.it Tel: +39 02 2399 8590 Fax: +39 02 2399 8585

Optical characterization of laser coloured titanium under different processing atmospheres

Noor Yasir Khafaji¹, Ali Gökhan Demir^{2,*}, Luigi Vitali³, Damiano Fustinoni³,

Alfonso Niro³, Barbara Previtali², Ziad A. Taha¹

¹ Institute of Laser for Postgraduate Studies, University of Baghdad, Baghdad, Iraq

² Department of Mechanical Engineering, Politecnico di Milano, Via La Masa 1, 20156 Milan, Italy

³ Energy Department, Politecnico di Milano, Via Lambruschini 4, 20156 Milan, Italy

Abstract

In this work, laser colouring of commercially pure Ti (grade II) samples under three different gas atmospheres is shown and analysed. The laser colouring process was carried out by means of a ns-pulsed Yb-fiber laser operating at a wavelength of 1064 nm with a pulse duration of 250 ns, while the process gas composition was controlled by mixing an inert gas, i.e. argon, with oxygen in different proportions; the results are compared with the same processing in ambient air atmosphere. Colour appearance based on the interference phenomenon in a thin oxide film is explained with a simple analytical model. Hemispherical reflectance spectra of coloured specimens were measured in the visible wavelength range, and, from them, chromaticity values were calculated. The results showed that the employed gas mixtures increased the oxide layer thickness, allowing for a more rapid colour transformation. The annulled wavelength, expressed by the lowest reflectance wavelength, moved from near-ultraviolet region towards near-infrared with increased fluence, as expected from the interference model. Oxide thicknesses of specimens with different colours were measured to validate the analytical model, which was found to predict in a satisfactory manner the lowest reflectivity wavelengths in the visible spectrum.

Keywords: Titanium colouring; optical properties; interference; reflectance spectroscopy.

1. Introduction

Oxide layers of titanium and its alloys exhibit variety of vivid colours in visible spectrum [1]. This type of permanent colouring is highly appealing for both aesthetic and technical purposes [2]. Various methods

exist to obtain a titanium oxide layer, namely, electrolytic oxidation (anodizing) [3], magnetron sputtering [4], thermal oxidation [5], cathodic deposition [6], plasma deposition [7] and laser deposition [8]. As a thermal source, laser provides a more flexible, precise and selective tool to obtain these layers with a high dimensional precision on metallic surfaces [9-17].

During the laser colouring process, titanium reacts mainly with oxygen to produce a semi-transparent coating [9]. Different laser can be employed such as pulsed CO₂ laser [10], pulsed solid state Nd:YAG laser [11,12], and fiber laser [13,14,15], where solid state lasers provide higher precision due to their smaller beam dimension. Several parameters related to the laser source and scanning strategy are used to control the energy delivered to the material surface [17]. These parameters directly affect phase, microstructure, and thickness of the oxide layer, which generates the variation of the perceived colour [18].

Two different main optical mechanisms are identified as responsible for the generation of colours, i.e. interference and absorption [19]. Concerning the interference phenomenon, the colour variation is linked mainly to the oxide thickness. On the other hand, the chemical composition of the oxide layer can vary the refractive index, and hence the absorption properties of the transparent layer. The processing atmosphere, and especially its chemical composition, is an important aspect for the process, since it can vary the thickness as well as the chemical composition of the oxide layer. Evidently, the effect of a processing atmosphere variation on the laser colouring process requires further attention in terms of optical properties of the obtained layers. Furthermore, linking the optical properties to an analytical solution of the interference phenomenon can provide the means to predict the behaviour of colour formation as a function of the process parameters.

In this work, laser colouring of commercially pure titanium (grade II) was studied employing a ns-pulsed fiber laser with several operating parameters. In particular, the same laser colouring process was carried out in ambient air, as well as under two different atmospheres, controlled by different mixtures of inert (Ar) and reactive (O₂) gas flows. Hemispherical reflectance spectra in the visible wavelength range were measured with a spectrophotometer equipped with an integrating sphere, to evaluate the coloured patches

chromaticity. A simple analytical model is provided to explain colour appearance based on interference occurring in thin oxide film; the experimental values of the wavelength corresponding to the lowest reflectivity as well as of the oxide thicknesses were compared to the analytical predictions.

2. Analytical modelling of interference in thin oxide films

A simple analytical solution to predict the visible colour reflected by the surface based on the interference phenomenon can be written by considering ray optics [20]. As shown in Figure 1, when an incident light ray (I) arrives at the surface of the oxide layer it is in part reflected (R_1) and in part transmitted (T_1) through the oxide layer. The transmitted ray is reflected at the oxide layer/bulk material interface (RT_1), which is transmitted back to air passing through the oxide layer/air interface. The optical path difference (Δp) between the two rays R_1 and TRT_1 determines whether destructive or constructive interference can occur, and it depends on the refraction angle determined by Snell's law (ϑ_2) [8], the oxide layer thickness (t), and the oxide layer refractive index (n_2), the latter depending in turn on the wavelength (λ):

$$\Delta p = 2 \cdot n_2(\lambda) \cdot t \cdot \cos \vartheta_2$$

Eq. 1

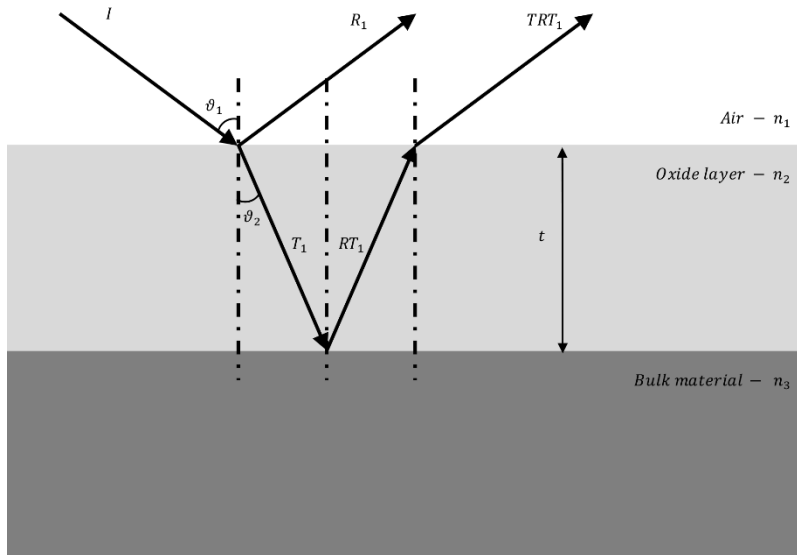


Figure 1. Schematic representation of the interference phenomenon occurring between the light ray reflected from the oxide layer surface and another ray that passes through the oxide layer.

For constructive interference, the optical path difference must be equal to an integer multiple (m) of a given wavelength (λ), whereas for destructive interference the optical path difference must be an integer multiple of a half wavelength ($\lambda/2$). As a result of the destructive interference, a certain wavelength band within the incident white light will be annulled, and the remaining band will be perceived as a resulting colour. For a system consisting of three layers with different refractive indices as seen in Figure 1, where $n_1 < n_2 < n_3$, Eq. 1 can be rewritten for constructive and destructive interference.

$$\begin{cases} m \cdot \lambda = 2 \cdot n_2(\lambda) \cdot t \cdot \cos \vartheta_2 \Rightarrow \text{constructive interference} \\ \left(m - \frac{1}{2}\right) \cdot \lambda = 2 \cdot n_2(\lambda) \cdot t \cdot \cos \vartheta_2 \Rightarrow \text{destructive interference} \end{cases} \quad \text{Eq. 2}$$

Eq.2 can be rewritten to calculate the thickness required to eliminate a certain wavelength:

$$t = \frac{\left(m - \frac{1}{2}\right) \cdot \lambda}{2 \cdot n_2(\lambda) \cdot \cos \vartheta_2} \quad \text{Eq. 3}$$

Eq.3 states that the same wavelength can be annulled with different oxide thicknesses as m increases. This also means that different wavelengths can be annulled with the same oxide thickness.

3. Material and methods

3.1 Material

Commercially pure titanium (grade II) was used throughout the work. The material was cold rolled to 0.3 mm thickness. Initial average surface roughness was measured as $Sa = 68.6 \pm 10$ nm. Before the experiments, the plates were cleaned in ethanol.

3.2 Laser system

A ns-pulsed fiber laser operating at a wavelength of 1064 nm was used (YLP-1/100/50/50 from IPG Photonics, Cambridge, MA, USA). The laser produced pulses with 250 ns duration, operating between 20 and 80 kHz. A galvanometric scanner head was used for beam manipulation (TSH8310 from Century

Sunny, Beijing, China). The scanner housed a 100 mm focal length f-theta lens. In this configuration, the spot size at the focal plane is 39 μm . Polarization state of the beam was random. A custom-made gas chamber was used to create a processing environment with a controlled atmosphere. The chamber had a top glass aperture transparent in the laser operating wavelength, while the process gases flows were controlled using separate flowmeters and mixed before being injected in the chamber. Argon with 99.998% purity was used as the inert gas, while oxygen with 99.95% purity was the reactive one. A continuous flow was used during the colouring experiments, which maintained gas mixture at desired composition and presumably contributed to the cooling of the surface due to convection. Static conditions were not employed, to avoid complete separation of the mixed gasses due to the difference in their densities. It can be expected that in static conditions, Ar can accumulate at the bottom of the chamber deviating the oxygen content from the desired one and eventually forming an inert barrier. A schematic representation of the experimental setup is shown in Figure 2.

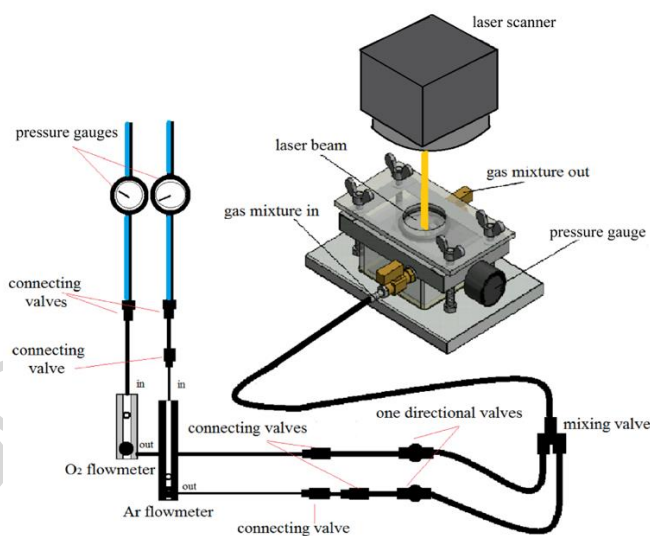


Figure 2. Schematic representation of the system used for sample laser treatment under an atmosphere of argon and oxygen.

3.3 Optical, chemical and microscopic characterization

A UV-Vis-NIR spectrophotometer equipped with a 150 mm Spectralon integrating sphere (Lambda 950 from Pelkin Elmer, Waltham, MA, USA) was used to characterize the optical properties of the coloured

surfaces. The characteristics of the experimental setup and its use in a similar application is detailed elsewhere [21]. In detail, hemispherical reflectance spectra have been acquired in a wavelength range from 380 nm to 780 nm, in steps of 10 nm. The interrogating beam size on the sample have been reduced to 9 mm x 9 mm by means of the internal Common Beam Mask, in order to fit into the 10 mm x 10 mm coloured areas. Chromaticity was evaluated from the acquired spectra; the CIE 1931 photonic observer and D65 illumination standards were implemented for analysis.

Average surface roughness (S_a) was measured with focus variation microscopy (Infinite Focus from Alicona, Graz, Austria). Images were acquired using 100X objective. The image field was 146 x 111 μm^2 . Estimated vertical and lateral resolutions were 0.005 μm and 1.5 μm respectively. Roughness profile was obtained using a Gaussian filter applied on the height maps with cut off frequency at 29.14 μm . Chemical composition was analysed using energy dispersive spectroscopy (EDS, Quantax/QX2 from Bruker, Billerica, MA, USA). Surface chemistry was analysed with a sensing depth up to 5 μm . Such depth is larger than the oxide thicknesses reported in the literature (<1 μm), allowing to assess the fraction of oxidation from surface to the material bulk [22,23]. SEM images were taken on the cross-section of the oxide zone.

Table 1. Details and results of the experimental campaign.

No.	E / mJ	PRR / kHz	v / mm s ⁻¹	h / μm	F _a / J cm ⁻²	% O ₂	v/v	S _a / nm	L*	a*	b*
1	0.1		200		175	21		88±23	61.79	1.95	13.75
2	0.1		170		206	21		85±16	37.29	17.29	13.92
3	0.1		140		250	21		88±23	47.25	13.20	34.11
4	0.16	35	200	10	280	21		78±8	60.29	4.02	22.71
5	0.16		170		329	21		65±8	43.59	-2.01	-12.37
6	0.16		140		400	21		77±11	26.88	-2.10	-21.36
7	0.1		200		175	57		50±2	63.35	2.28	17.40
8	0.1		170		206	57		50±5	32.68	21.67	13.84
9	0.1		140		250	57		75±44	44.77	14.95	35.65
10	0.16	35	200	10	280	57		65±10	59.71	4.74	27.47
11	0.16		170		329	57		58±3	47.76	-1.14	-7.10
12	0.16		140		400	57		48±4	34.15	-2.51	-20.26
13	0.1		200		175	80		62±6	61.80	2.35	17.30
14	0.1	35	170	10	206	80		58±4	27.23	7.79	-13.14
15	0.1		140		250	80		47±6	38.76	17.52	18.16

16	0.16	200	280	80	54±1	53.32	8.18	31.02
17	0.16	170	329	80	50±20	51.50	-0.61	-4.06
18	0.16	140	400	80	58±18	47.56	-1.77	-8.39

3.4 Experimental plan

The laser colouring process consists of overlapping laser pulses in a scan direction and adjacent scan lines. The amount of energy released on the material surface is controlled by the laser pulse energy (E), scan speed (v), hatch distance between adjacent scan lines (h), and pulse repetition rate (PRR). Focal position was fixed 2 mm above the material surface. In this configuration, the beam diameter was enlarged to 124 μm . Two levels of pulse energy, i.e. 0.10 and 0.16 mJ, were used, whereas the pulse repetition rate was fixed at 35 kHz. The scan speed was varied between 140, 170 and 200 mm/s. The experiments were carried out in three different processing atmospheres, namely in ambient air (assumed 21% v/v O_2), under 15 NL/min Ar + 20 NL/min O_2 (57% v/v O_2) and under 5NL/min Ar + 20 NL/min O_2 (80% v/v O_2). A 10 mm x 10 mm patch has been generated for each combination of the process parameters, as detailed in Table 1. The results were analysed also as a function of areal fluence. Areal fluence (F_a) can be expressed as the fraction of total energy (E_{tot}) over total scanned area (A_{tot})

$$F_a = \frac{E_{tot}}{A_{tot}} \quad \text{Eq. 4}$$

For a generic square shaped area with l_1 and l_2 lengths, the expression becomes

$$F_a = \frac{E \cdot N_{tot}}{A_{tot}} = \frac{E \cdot \frac{l_1 \cdot PRR \cdot l_2}{v}}{l_1 \cdot l_2} \quad \text{Eq. 5}$$

where N_{tot} is the total number of pulses released on the scanned area. Simplifying this expression, the final form is obtained as:

$$F_a = \frac{E \cdot PRR}{v \cdot h} \quad \text{Eq. 6}$$

The Eq.4 differs from the more common definition of fluence as the peak energy density of the laser beam [24]. While not considering the beam shape, the expression is capable of comparing the energy released to the unit area as a function of scan speed and hatch distance. Since experimental conditions

employed the same focal position and hence the same beam size, for comparative purposes areal fluence was preferred.

4. Results and discussion

The colours obtained under different processing conditions are shown in Figure 3, while colorimetric coordinates $L^*a^*b^*$ are listed in Table 1 along the corresponding processing parameters. It can be observed that colour formation starts from a faint yellow and moves toward shades of red, then to shades of blue and finally to a light blue/gray combination as the oxidized layer increases, due to the combination of a fluence increase and a more reactive atmosphere. The results also depict that average surface roughness remains at a range comparable to that of the as-received sample surface. The surfaces obtained in ambient air result to have slightly higher average roughness values. Figure 4 exhibits the SEM images of the coloured surfaces. The images show compact and homogenous surface structure with a small fraction of micrometric cracks when processing under ambient air. These cracks are expected to be formed due to the rapid heating and cooling cycles induced within the process [25]. The use of gas mixtures appears to reduce the crack formation, presumably due to the surface cooling provided by convection. The surfaces did not show any periodic surface structures in nanometric scale capable of producing colours in the visible range by diffraction [26]. As a matter of fact, colours generated due to diffraction effects are sensitive to the orientation of the periodic structures with respect to the viewing angle, which is not the case in colours generated by a compact oxide layer. Cold interaction with ultrafast pulses and controlled polarization states are the prerequisites of generating diffractive surface structures, which are absent in the proposed treatment.

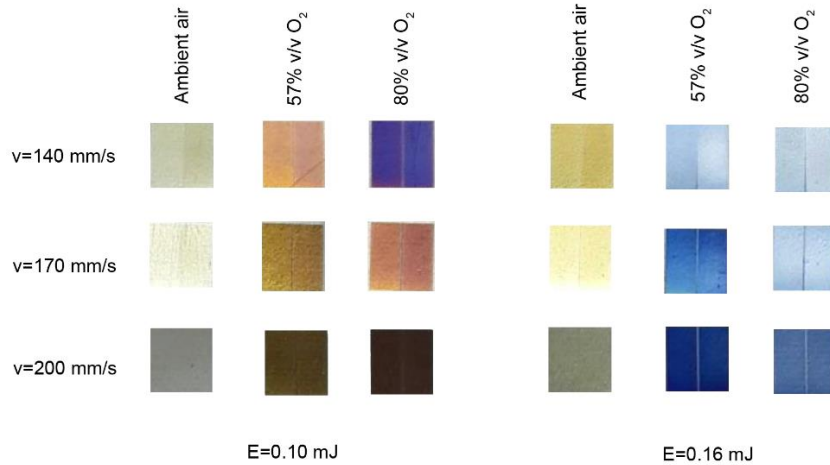


Figure 3. Coloured specimens obtained with different processing conditions.

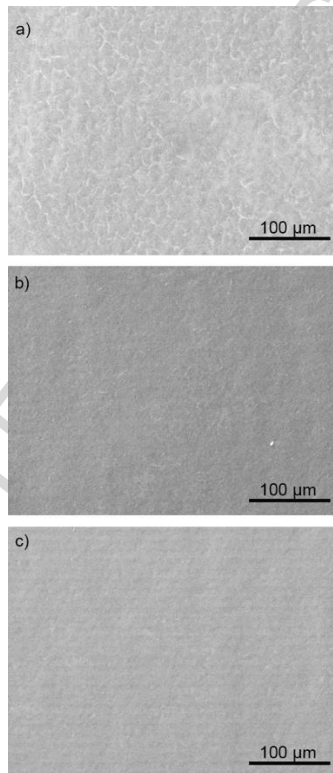


Figure 4. SEM images of the coloured samples showing surface topography obtained under a) ambient air; b) 57% v/v O₂; c) 80% v/v O₂ (v=170 mm/s; E=0.16 mJ).

Figure 5 displays the hemispherical visible reflectance spectra of the selected parameter combinations. As it can be observed from the images, increasing the pulse energy and decreasing the scan speed generates stronger colour changes while operating under high-oxygen gas mixtures with respect to ambient air. The corresponding reflectance spectra show that the faint grey and yellow observed when operating in

ambient air correspond to spectra characterized by a decaying reflectivity towards ultraviolet range. These spectra show high reflectivity around 730-780 nm. In a high-oxygen environment, the reflectivity for the minimum fluence conditions increases near the ultraviolet range, shifting the lowest reflectivity point towards the centre of the visible range. The colours appear in the tones of dark yellow and orange. With increased pulse energy and decreased scan speed, the spectra lowest point moves further towards the near infrared range, while the band between 380 and 480 nm increases. The colours appear in the shades of blue. The parameter conditions producing fluences close to ablation region appear in lighter shades of blue. The parameter conditions producing fluences close to ablation region appear in lighter shades of blue, such as the ones obtained with $E = 0.16$ mJ, $v = 170$ mm/s and $E = 0.16$ mJ, $v = 140$ mm/s under an 80% v/v O_2 atmosphere. As a consequence, the reflectance spectra are overall shifted to a higher reflectivity range compared to the other shades of blue. Figure 5 shows the lowest reflectivity wavelengths as a function of areal fluence for the three tested processing atmospheres. It can be seen that operating under gas mixtures provides a stronger change as a function of fluence. On the other hand, for all processing atmospheres, the increase of areal fluence results in shifting the minimum reflectivity point towards NIR.

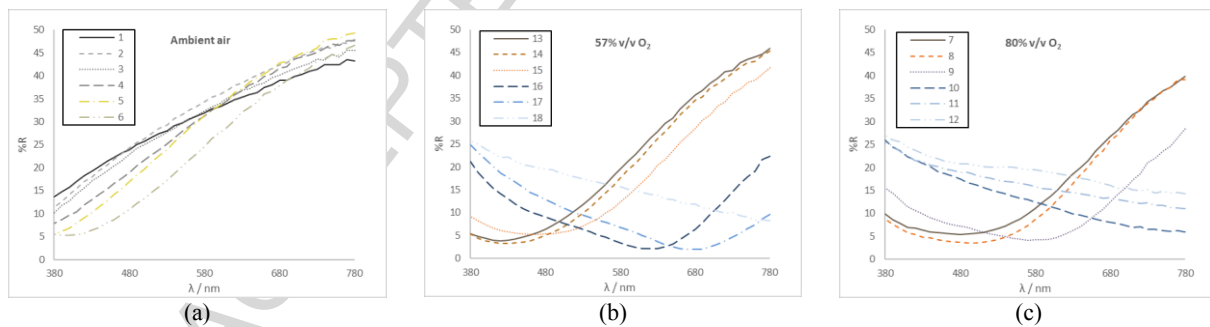


Figure 5. Reflectance spectra of the coloured samples, respectively under ambient air (a), a 57% v/v O_2 (b) and a 80% v/v O_2 atmosphere (c). Numbers in the legend refer to the machining conditions listed in Table 1. Line colours are only indicative of the actual surface colour.

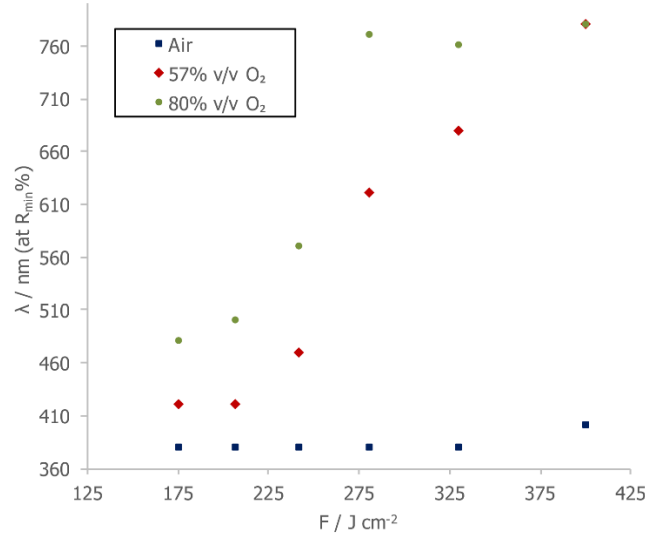


Figure 6. Lowest reflectance wavelength as a function of fluence, for the three different processing atmosphere conditions.

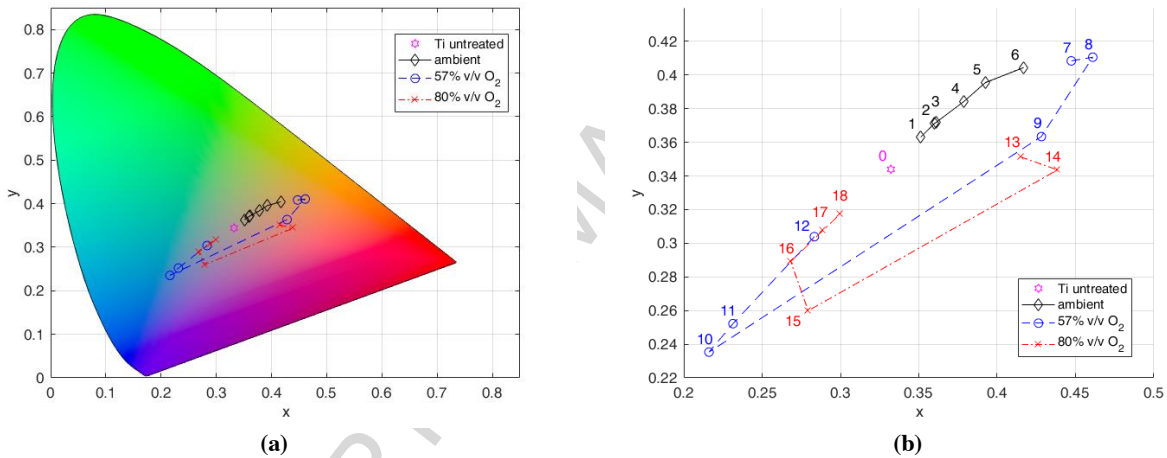


Figure 7. Chromaticity values for the resulting coloured surfaces in different atmospheres plotted over the CIE1931 colour space (a), and zoom of the same plot (b), with numbers referring to the laser machining parameters listed in Table 1. The untreated titanium sample chromaticity is also shown as reference (0).

Figure 6 displays the chromaticity values of the selected conditions. The position of the results on the chromaticity diagram confirms the capacity of using the gas mixtures in generating a wider range of colours. In the same fluence region ($F_a=175-400 \text{ J/cm}^2$), the colours obtained in ambient air remain as variants of yellow. The colours move towards the orange range as the fluence increases following a linear path, as also observed in the qualitative analysis. On the other hand, when operating under a 57% v/v O_2 atmosphere, the colours appears around $x = 0.45, y = 0.41$ for the smallest fluence ($F_a = 175 \text{ J/cm}^2$). As the fluence increases, the new colours appear first at an adjacent coordinate around $x = 0.46, y = 0.41$ (F_a

= 206 J/cm²) and then move towards to the other extreme of the chart around $x = 0.22$, $y = 0.24$ ($F_a = 280$ J/cm²). An increase on both coordinates is associated with a fluence increase after this point. Such behaviour is also present in an 80% v/v O₂ atmosphere. With the lowest fluence value ($F_a = 175$ J/cm²) the colour coordinates are $x = 0.42$, $y = 0.35$, which move to $x = 0.44$, $y = 0.34$ with $F_a = 206$ J/cm². After this point, the increase of fluence moves the coordinates to $x = 0.28$, $y = 0.26$. It is noteworthy that both the colouring processes in oxygen-rich atmospheres show a circular behaviour in the CIE1931 colour space, and that the processes carried out in the 80% v/v O₂ atmosphere anticipate some of the resulting colours of the 57% v/v O₂ atmosphere, i.e. samples 14 vs. 9 (light red), 17 vs. 12 (light blue), and the transition from reddish to blueish colours.

4.1 The missing green

It is interesting to observe that none of the trends move towards the green colour region. As a matter of fact, shades of green on titanium obtained by means of laser colouring have not been reported. From a spectral standpoint, a green surface should be composed of a peak around the centre of the visible spectrum with a low reflectance on the both ends.

Experimentally, it can be seen that the reflectance spectra maxima and minima shift from near-infrared to near-ultraviolet as the energy input increases. Such phenomenon fits well with the interference model for colour generation, as described in section 2. According to this model, the annulled wavelength λ_a (or the wavelength with the lowest reflectivity) increases as a function of the oxide layer thickness t , which in turn increases with the laser fluence and, as tested, with the oxygen content of the processing atmosphere, until a maximum value for a fixed integer multiple m . The lowest point of the reflectance band starts near the ultraviolet region and moves towards the infrared region. This behaviour is then cycled to increase values of m , with the addition of more than one value of λ_a as t increases, as shown in Figure 8 by solving Eq. 3.

In order to obtain a reflectance peak around the centre of the visible bandwidth, so to obtain green colour, it would be required to eliminate wavelengths around both near-ultraviolet and near-infrared. This problem can be resolved rewriting Eq.3 for the visible spectrum extremities:

$$t = \frac{(m_1 - \frac{1}{2}) \cdot 380}{2 \cdot n_2(\lambda = 780 \text{ nm}) \cdot \cos \vartheta_2} = \frac{(m_2 - \frac{1}{2}) \cdot 780}{2 \cdot n_2(\lambda = 380 \text{ nm}) \cdot \cos \vartheta_2} \quad \text{Eq. 7}$$

Using refractive index values from Ref. [23], n_2 was estimated as 2.47 and 2.05 for 380 nm and 780 nm respectively. A close solution is present when $m_1 = 14$ and $m_2 = 6$, indicating an oxide thickness close to 1040 nm. In such thickness values, the interference phenomenon is less likely to occur with white light, which is characterised by very low coherence. Moreover, such oxide thickness is hard to achieve and would be instable also due to its high fragility. With an increase in thickness, absorption is also expected to play an important role, by decreasing the intensity of the light transmitted through the oxide layer.

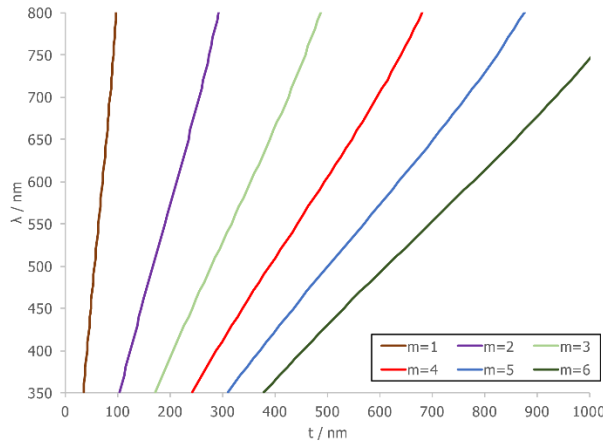





Figure 8. Annulled light wavelength as a function of oxide thickness. The values were calculated using refractive index data from [23], for an incident beam perpendicular to the surface ($\vartheta_2 = 0^\circ$)

4.2 Chemical composition and oxide thickness

Chemical composition was evaluated on chosen specimens corresponding to a single set of laser parameters ($E = 0.16$ mJ, $v = 200$ mm/s, $h = 0.01$ mm, $F = 280$ J/cm²) with different processing atmospheres. Table 2 reports the chemical composition of the oxide layers measured by EDS. It can be observed that the oxygen amount increases significantly with the use of gas mixtures, moving oxygen content from around 20 wt% to 40 wt% despite the increased scan speed. Figure 9 shows SEM images of the cross sections of the oxide layers obtained under gas mixtures. The layer thicknesses were estimated

from these images, and it can be observed that, by increasing the oxygen percentage in the processing atmosphere, the thickness could be increased from 298 nm to 793 nm. Both thicknesses are expected to generate destructive interference around the central zone of the visible and near infrared spectral bands according to Eq.4 and as demonstrated in Figure 8. The remaining band corresponds to reflectance peaks around the blue wavelength, which is consistent with the observed specimen colours (Figure 3) and with the measured reflectance spectra (Figure 5).

Table 2 Influence of processing atmosphere on the chemical composition and the thickness of the oxide layers ($E = 0.16$ mJ, $v = 200$ mm/s, $h = 0.01$ mm).

Colour	Processing atmosphere	O wt%	N wt%	C wt%	Ti wt%	t / nm
	Air	20.4	20.4	5.8	57.6	<100
	57% v/v O ₂	36.6	12.5	3.8	47.2	298
	80% v/v O ₂	39.9	11.6	3.5	45.0	703

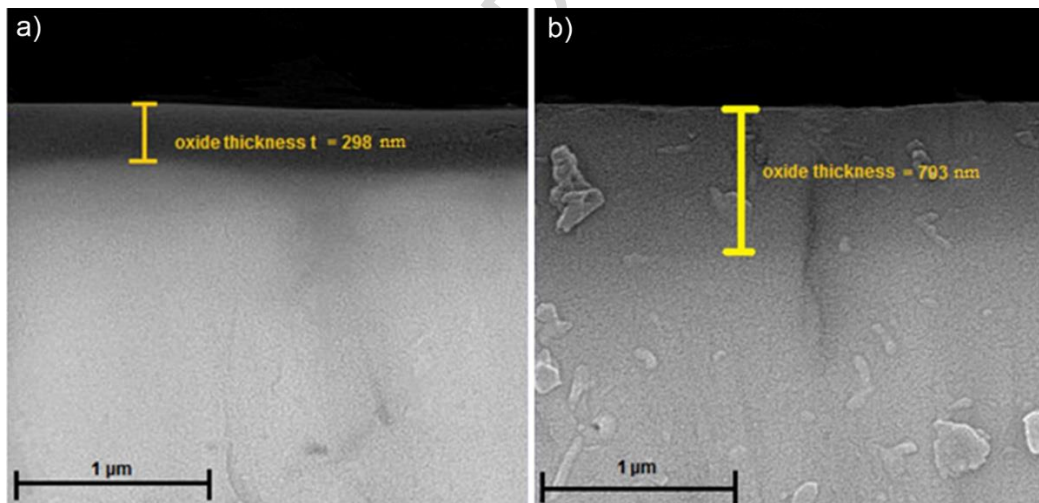


Figure 9. SEM images showing the oxide layers. a) 57% v/v O₂, b) at 80% v/v O₂.

5. Conclusions

This work shows the results of laser colouring processes on titanium samples under two oxygen-rich controlled atmospheres, respectively with 57% and 80% v/v O₂. The resulting colours show major

differences with the ones obtained under atmospheric air for the same laser operating parameters, mainly due to the increased thickness of the surface oxide layer. In particular, the hemispherical reflectance spectra of the resulting colours revealed that the minimum reflectance wavelength moved from the near-ultraviolet region towards the near-infrared as laser fluence and oxygen content in the atmosphere increased. The corresponding colour coordinates were calculated, and a rotating behaviour was observed. Moreover, the colour-changing trends did not show any projections towards the shades of green, which is a colour that is not easily obtained on titanium by laser oxidation. To further investigate this behaviour, an analytical model of the optical interference between light rays reflected from the surface and delayed ones by transmission inside the oxide layer was implemented, and the oxide thickness required to generate green shades has been calculated. The resultant value is in the range of micrometers, depicting the difficulty in obtaining this colour by interference. Finally, a verification of the model has been made by showing its ability to predict the wavelengths of the lowest reflectivity as a function of oxide layer thickness. This data is consistent with the oxide layer thickness measurement by means of SEM, in cross section images, and with the observed resulting colour.

Acknowledgments

The authors gratefully acknowledge Iraqi Ministry of Higher Education and Scientific Research, and the Institute of Laser for Postgraduate Studies, University of Baghdad for partially funding this research.

References

1. P. Pedferri, Drawings on Titanium, Clup, Milan, 1981
2. I. De Graeve, The road to intelligent coloured coatings, *Surface Eng.* 27(10) (2011) 719–723
3. M. V. Diamanti, B. Del Curto, M.P. Pedferri, Interference colors of thin oxide layers on titanium, *Color Res. Appl.* 33(3) (2008) 221-228.
4. J. H. Lee, G.E. Jang, G.E. Jang, Investigation and evaluation of structural color of TiO₂ coating on stainless steel, *Ceram. Int.* 38 (2012) 661–664
5. H. Dong, T. Bell, Enhanced wear resistance of titanium surfaces by a new thermal oxidation treatment, *Wear* 238 (2010) 131-137
6. H. Takikawa, T. Matsui, T. Sakakibara, A. Bendavid, P. J. Martin, Properties of titanium oxide film prepared by reactive cathodic vacuum arc deposition, *Thin Solid Films* 348 (1999) 145-151
7. K.S. Teng, J. L. Delplancke, J. Zhang, T.J. O’Keefe, Electrochemical Characterization of Copper Deposited on Plasma and Thermally Modified Titanium Surfaces, *Metal. Mater. Trans.* 29 (1995) 749-754
8. C. Garapon, C. Champeaux, J. Mugnier, G. Panczer, P. Marchet A. Catherinot, B. Jacquier, Preparation of TiO₂ thin films by pulsed laser deposition for waveguiding applications, *Appl. Surf. Sci.* 96-98 (1996) 836-841.
9. Ł. Skowrońska, A.J. Antończak, M. Trzcinski, Ł. Łazarek, T. Hiller, A. Bukaluka, A. A. Wronkowska, Optical properties of laser induced oxynitride films on titanium, *Appl. Surf. Sci.* 304 (2014) 107–114
10. S. O’Hana, A. J. Pinkerton, K. Shoba, A. W. Gale, L. Li., Laser surface colouring of titanium for contemporary jewellery, *Surf. Eng.* 24 (2008) 147-153.
11. L. Lavisse, M.C. Sahour, J.M. Jouvard, G. Pillon, M.C. Marco de Lucas, S. Bourgeois, D. Grevey, Growth of titanium oxynitride layers by short pulsed Nd:YAG laser treatment of Ti plates: Influence of the cumulated laser fluence, *Appl. Surf. Sci.* 255 (2009) 5515–5518

12. C. Langlade, A. B. Vannes, J. M. Krafft and J. R. Martin, Surface Modification and tribological behaviour of titanium and titanium alloys after YAG-laser treatments, *Surf. Coat. Tech.* 101 (1998) 383-387
13. J. Antończak, L. Skowroński, M. Trzcinski, V. Kinzhybalov, K. Łazarek, M. Abramski, Laser-induced oxidation of titanium substrate: Analysis of the physicochemical structure of the surface and sub-surface layers, *Appl. Surf. Sci.* 325 (2015) 217-226
14. D. P. Adams, R.D. Murphy, D.J. Saiz, D.A. Hirschfeld, M.A. Rodriguez, P.G. Kotula, B.H. Jared, Nanosecond pulsed laser irradiation of titanium: Oxide growth and effects on underlying metal, *Surf. Coat. Tech.* 248 (2014) 38-45
15. A. J. Antonczak, B. Stepak, P. E. Koziol, K. M. Abramski, The influence of process parameters on the laser-induced coloring of titanium, *Appl. Phys. A* 115 (2014) 1003-1013
16. H.Y. Zheng, H.X. Qian, W. Zhou, Analyses of surface coloration on TiO₂ film irradiated with excimer laser, *Appl. Surf. Sci.* 254 (2008) 2174-2178
17. D. P. Adams, R.D. Murphy, D.J. Saiz, D.A. Hirschfeld, M.A. Rodriguez, P.G. Kotula, B.H. Jared, Nanosecond pulsed laser irradiation of titanium: Oxide growth and effects on underlying metal, *Surf. Coat. Tech.* 248 (2014) 38-45
18. L. Lavis, J.M. Jouvard, L. Imhoff, O. Heintz, J. Korntheuer, C. Langlade, S. Bourgeois, M.C. Marco de Lucas, Pulsed laser growth and characterization of thin films on titanium substrates", *Appl. Surf. Sci.* 253 (2007) 8226-8230.
19. R. C. Gonzalez, R. E. Woods, *Digital Image Processing*, 2nd Ed, Tom Robbins, 2001.
20. F. Franceschini, A.G. Demir, J.D. Griffiths, C. Dowding, B. Previtali, Laser colouring on titanium alloys: characterisation and potential applications, *Proceedings of X Conferenza del Colore* (2014) 12 pp
21. L. Vitali, D. Fustinoni, P. Gramazio, H. Niro, Spectral BRDF measurements of metallic samples for laser processing applications, *J. Phys. Conf. Ser.* 665 (2015) 012064

22. A. Pérez del Pino, J.M. Fernandez-Pradas, P. Serra, J.L. Morenza, Coloring of titanium through laser oxidation: comparative study with anodizing, *Surf. Coat. Tech.* 187 (2004) 106-112
23. S. Van Gils, P. Mast, E. Stijns, H. Terryn, Colour properties of barrier anodic oxide films on aluminium and titanium studied with total reflectance and spectroscopic ellipsometry, *Surf. Coat. Tech.* 185 (2004) 303-310
24. K.M.T. Ahmmed, C. Grambow, A.-M. Kietzig, Fabrication of Micro/Nano Structures on Metals by Femtosecond Laser Micromachining, *Micromachines* 5 (2014), 1219-1253
25. E. Akman, E. Cerkezoglu, Compositional and micro-scratch analyses of laser induced colored surface of titanium, *Opt. Laser. Eng.* 84 (2016), 37-43
26. B. Dusser, Z. Sagan, H. Soder, N. Faure, J.P. Colombier, M. Jourlin, E. Audouard, Controlled nanostructures formation by ultra fast laser pulses for color marking, *Opt Expr* 18(3), (2010) 2913-2924

List of figures

Figure 1. Schematic representation of the interference phenomenon occurring between the light ray reflected from the oxide layer surface and another ray that passes through the oxide layer.

Figure 2. Schematic representation of the system used for sample laser treatment under an atmosphere of argon and oxygen.

Figure 3. Coloured specimens obtained with different processing conditions.

Figure 4. SEM images of the coloured samples showing surface topography obtained under a) ambient air; b) 57% v/v O₂; c) 80% v/v O₂ ($v=170$ mm/s; $E=0.16$ mJ).

Figure 5. Reflectance spectra of the coloured samples, respectively under ambient air (a), a 57% v/v O₂ (b) and a 80% v/v O₂ atmosphere (c). Numbers in the legend refer to the machining conditions listed in Table 1. Line colours are only indicative of the actual surface colour.

Figure 6. Lowest reflectance wavelength as a function of fluence, for the three different processing atmosphere conditions.

Figure 7. Chromaticity values for the resulting coloured surfaces in different atmospheres plotted over the CIE1931 colour space (a), and zoom of the same plot (b), with numbers referring to the laser machining parameters listed in Table 1. The untreated titanium sample chromaticity is also shown as reference (0).

Figure 8. Annulled light wavelength as a function of oxide thickness. The values were calculated using refractive index data from [23], for an incident beam perpendicular to the surface ($\theta_2 = 0^\circ$)

Figure 9. SEM images showing the oxide layers. a) 57% v/v O₂, b) at 80% v/v O₂.

List of tables

Table 1. Details and results of the experimental campaign.

Table 2 Influence of processing atmosphere on the chemical composition and the thickness of the oxide layers ($E = 0.16$ mJ, $v = 200$ mm/s, $h = 0.01$ mm).

ACCEPTED MANUSCRIPT

Highlights

- Laser colouring of titanium was applied under different process atmospheres.
- Inert Ar was mixed with reactive O₂ in different proportions and compared to processing in air.
- Reflectance spectra were acquired on the produced coloured patches.
- An analytical model was proposed linking oxide thickness to the annulled wavelengths.
- Oxide thickness measurements and perceived colours were consistent with the developed model.